JCTC Journal of Chemical Theory and Computation

Visualization of Molecular Orbitals and the Related Electron Densities

Maciej Haranczyk*,† and Maciej Gutowski*,†,‡

Department of Chemistry, University of Gdańsk, Sobieskiego 18, 80-952 Gdańsk, Poland, and Chemistry-School of Engineering and Physical Sciencs, Heriot-Watt University, Edinburgh EH14 4AS, U.K.

Received February 10, 2008

Abstract: When plotting different orbitals with consistent contour values, one can create illusions about the relative extension of charge distributions. We suggest that the comparison is not biased when plots reproduce the same fraction of the total charge. We have developed an algorithm and software that facilitate this type of visualization. We propose superimposing molecules and associated orbitals, and creating cross-sections by selecting a particular part of the orbital limited by pre-defined planes.

Molecular orbitals and the related electron densities are basic molecular features of interest to chemists. The values of electron density in a molecular fragment and the bonding/antibonding character of the orbital contribute to the chemical properties of this fragment. Therefore, practically all electronic structure codes give their users an option to access molecular orbital data, either in the form of the coefficients associated with basis functions or as volumetric data with values of the orbital or the related electron density at each point of a predefined grid. Many programs have been developed to visualize orbitals and/or electron density, and they are in common use by the community of computational chemists.[1–3] Orbitals and electron densities are typically visualized as finite volumes limited by a boundary defined by a preselected contour value (CV). On occasion, 2D maps, which are cross-sections of the finite volumes, are prepared with marked isovalues of the presented quantity.

Interestingly, plotting an orbital or electron density with a predefined contour value seems to be the only option implemented in the major visualization software packages.[1–3] Similarly, when comparing molecular orbitals or electron densities of different systems, one usually prepares plots using consistent

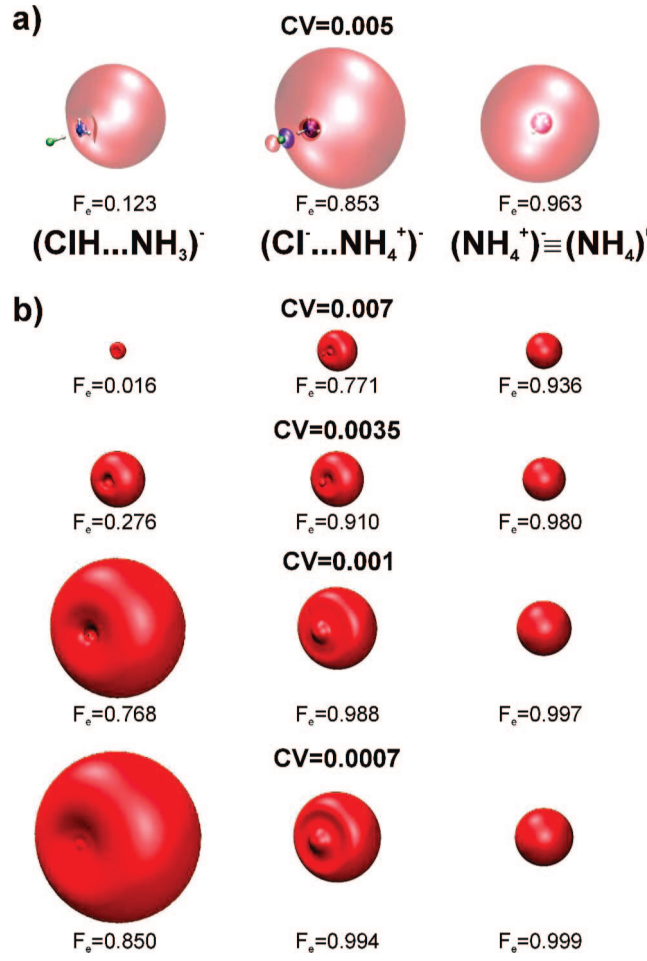

Figure 1. (a) Singly occupied molecular orbitals of the dipole-bound intermediate $(ClH\cdots NH_3)^-$ (left), the proton-transferred species $(Cl^-\cdots NH_4^+)^-$ (center), and, for comparison, the neutral Rydberg radical (NH_4^0) (right). The orbitals were plotted using a contour value (CV) of 0.005 bohr$^{-3/2}$. (b) Positive part of the orbital (pink in part a)) plotted with different CVs (in bohr$^{-3/2}$).

CVs. This approach works well when the charge distributions do not differ much in their spatial extension. We found, however, the same approach to be misleading when the studied charge distributions span a broad range of extension. The problem becomes particularly relevant when dealing with orbitals, which are characterized by very different orbital energies, and therefore different electron binding energies. This results from the long-range asymptotic behavior of bound-state wave functions and orbitals:[4,5] e.g., the occupied Hartree–Fock orbitals decay as $\exp[-(-2\varepsilon_{HOMO})^{1/2}r]$,[4] where ε_{HOMO} is the orbital energy of the highest occupied orbital. Here we will focus

* To whom correspondence should be addressed. E-mail: maharan@chem.univ.gda.pl (M.H.); m.gutowski@hw.ac.uk (M.G.).
† University of Gdańsk.
‡ Heriot-Watt University.

10.1021/ct800043a CCC: $40.75
Published on Web 04/05/2008

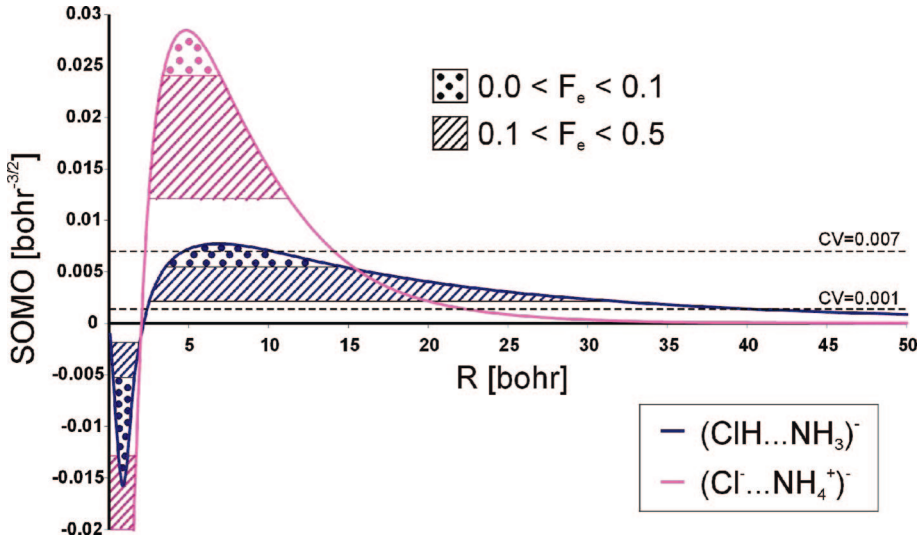

Figure 2. Decay of the SOMO orbitals. *R* defines the distance from N along the N−Cl line in the direction of the main lobes of the SOMOs.

on molecular anions, though the visualization of orbitals for neutral and cationic species encounters similar problems, e.g., when comparing Rydberg and valence orbitals of neutral species.

We will use two examples from our recent studies on molecular anions: an anionic complex of ammonia and hydrogen chloride,[6] and tautomers of an anionic nucleic acid base, guanine.[7–10] The selected systems cover various types of molecular anions: a dipole-bound anion,[6] a related system, in which a closed-shell anion is bound to a neutral Rydberg molecule,[6] and valence anions.[7–10]

The complex of ammonia and hydrogen chloride has been a subject of our recent study.[6] The neutral system has a hydrogen-bonded ($ClH\cdots NH_3$) structure in the gas phase.[11,12] Since it has a dipole moment of ca. 4.15 D, it supports a dipole-bound state with the excess electron attached to NH_3 (Figure 1a, left), and the calculated electron vertical attachment energy is 0.03 eV.[6] The excess electron attachment modifies the potential energy surface of ($ClH\cdots NH_3$) and promotes an intermolecular proton transfer, with the global anionic minimum having the $(Cl^-\cdots NH_4^+)^-$ form (Figure 1a, middle), and the excess electron remains bound to the nitrogen site, but with a much larger binding energy, 0.51 eV.[6] The latter anionic complex can also be characterized as a Rydberg radical, $(NH_4)^0$ (Figure 1a, right), polarized by Cl^-. The isolated, fully symmetric $(NH_4)^0$ radical is characterized by a vertical ionization potential of 5.08 eV.[6]

The significant differences in electron binding energies among $(ClH\cdots NH_3)^-$, $(Cl^-\cdots NH_4^+)^-$, and $(NH_4)^0$ should be reflected in the diffuseness of the singly occupied molecular orbital (SOMO). The corresponding SOMOs are presented in Figure 1a and were prepared according to the common practice—a consistent CV of 0.005 $bohr^{-3/2}$ was selected. Surprisingly, the SOMO of $(Cl^-\cdots NH_4^+)^-$ seems to be more diffuse than that of $(ClH\cdots NH_3)^-$, even though the former is characterized by an electron binding energy 1 order of magnitude larger than the latter. Below we demonstrate how this illusion develops and how to avoid it.

In Figure 1b we plotted bulky parts of the SOMOs using different contour values: 0.007, 0.0035, 0.001, and 0.0007 $bohr^{-3/2}$. For CV = 0.007 $bohr^{-3/2}$ the orbital bulb of $(ClH\cdots NH_3)^-$ is much smaller than for $(Cl^-\cdots NH_4^+)^-$ or $(NH_4)^0$. However, the opposite size relation might be deduced for CV = 0.0007 $bohr^{-3/2}$. Clearly, the visualization of molecular orbitals with the same CV value might fail to provide information about their relative sizes.

Table 1. Algorithm for Determination of a Contour Value Corresponding to a Preselected Fraction of the Total Orbital Charge

1. generate or read-in grid points and the corresponding volumetric data containing orbital or orbital density values
2. if the orbital values are provided in point 1, calculate the corresponding orbital density values
3. sort grid points according to the orbital density values
4. loop over sorted grid points and perform numerical integration of the orbital density starting from the point of the highest density value
5. stop integration when the integrated value exceeds the preselected fraction
6. the searched CV is equal to the value of orbital density at the last integrated point (if plotting electron densities) or to the properly signed square root of it (if plotting orbitals)

An important observation is that the fractions of electrons (F_e) contained in the volumes determined by the same CV value might be very different (Figure 1). For example, the SOMOs presented in Figure 1a reproduce 12.3% of e for $(ClH\cdots NH_3)^-$, 85.3% for $(Cl^-\cdots NH_4^+)^-$ and 96.3% for NH_4^0. Moreover, it requires quite a small CV value to reproduce a significant fraction of e for $(ClH\cdots NH_3)^-$. We conclude that the inability to derive information about the relative orbital sizes is related to the inconsistent F_e values.

To illustrate the point further, we show in Figure 2 plots of the SOMO for $(ClH\cdots NH_3)^-$ and $(Cl^-\cdots NH_4^+)^-$ as a function of *R*, where *R* is the distance from the nitrogen atom along the Cl−N line in the direction of the main lobes. The SOMO of $(Cl^-\cdots NH_4^+)^-$ decays much faster than that for $(ClH\cdots NH_3)^-$, as anticipated from the electron binding energies.[4] Both orbitals are normalized to 1, and therefore the maximum value of SOMO for $(ClH\cdots NH_3)^-$ must be smaller than for $(Cl^-\cdots NH_4^+)^-$. Consequently, if the CV is sufficiently large, then the criterion SOMO(*R*) > CV is met only for small values of *R* for $(ClH\cdots NH_3)^-$ but for larger *R* values for $(Cl^-\cdots NH_4^+)^-$. This

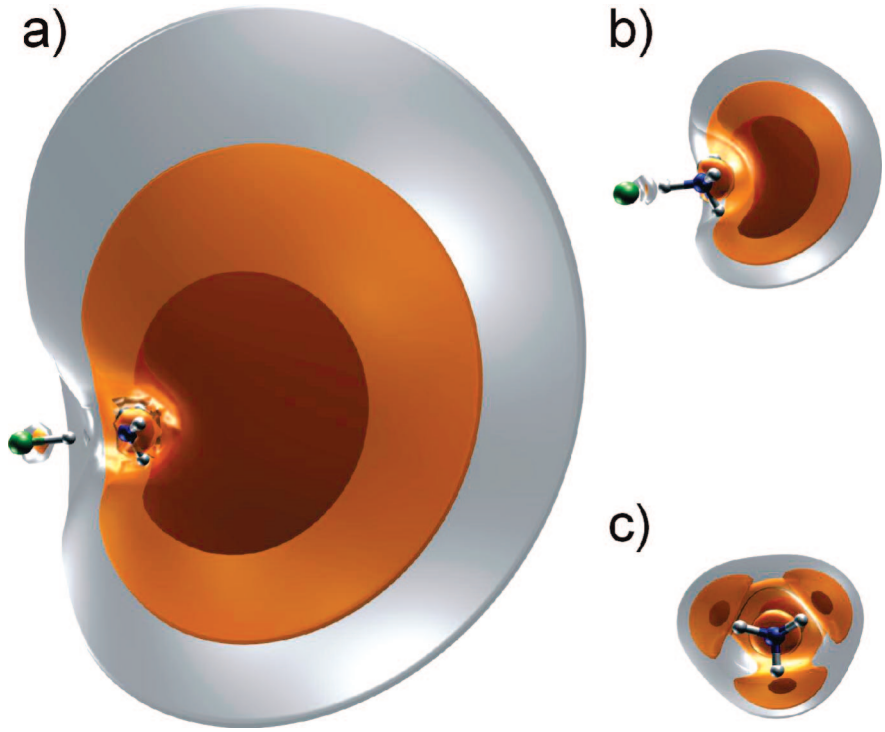

Figure 3. Cross-sections through the density of the SOMO for (a) the dipole-bound intermediate $(ClH\cdots NH_3)^-$, (b) the proton-transferred species $(Cl^-\cdots NH_4^+)^-$, and for comparison, (c) the neutral Rydberg radical (NH_4^o). These plots were generated with VMD[1] and OpenCubMan,[16] and the resulting contours enclose 0.1, 0.3 and 0.5 e from the inner to the outer shell, respectively.

explains why the plotted orbital is larger for $(Cl^-\cdots NH_4^+)^-$ than for $(ClH\cdots NH_3)^-$ for CV = 0.007 and 0.005 bohr$^{-3/2}$ (Figure 1). We re-emphasize that in these cases only small fractions of e are reproduced for $(ClH\cdots NH_3)^-$, whereas the F_e values exceed 0.7 e for $(Cl^-\cdots NH_4^+)^-$. It requires quite a small value of CV to have the SOMO of $(ClH\cdots NH_3)^-$ described by a lobe larger than that for $(Cl^-\cdots NH_4^+)^-$,: see the cases of CV = 0.001 and 0.0007 bohr$^{-3/2}$ in Figures 1 and 2. In these cases the F_e values exceed 0.7 e for all three systems.

In Figure 2 we also visualize these ranges of R that have to be included to reproduce a given value of F_e, and the two illustrated cases are $F_e = 0.1$ and 0.5 e. If the orbital plots were based on the criterion of the same value of F_e, then the SOMO of $(ClH\cdots NH_3)^-$ would be more diffuse than that for $(Cl^-\cdots NH_4^+)^-$. This suggests that an unbiased way to visualize orbitals or electron densities that differ much in the extension of charge distributions would be to ensure that a consistent and preselected fraction of the total charge is reproduced in each plot. The same conclusion was reached by Rauk and Armstrong in their studies of dipole-bound and valence anions in clusters involving various hydrogen halides.[13–15] The approach, i.e., plotting different orbitals in such a way that the same fraction of electron charge is reproduced, leads to another question: what are the CV's that lead to the same and preselected F_e's? Clearly, these CV's might be different for different orbitals. Here we present an efficient algorithm to determine the desirable CV's. The same algorithm can be used to calculate a fraction of the total charge corresponding to a particular CV. We also suggest how to graphically present information about the relative diffuseness of orbitals. First we make a list of a few F_e's, and we create all the 3D orbital plots for the preselected F_e's. Finally, for each orbital we superimpose plots corresponding to the preselected F_e's and we create 2D cross-sections that unravel information about the relative orbital diffuseness.

The proposed approaches are made available to the scientific community by providing appropriate software.[16] This software works with volumetric data containing orbitals or orbital densities. The latter are often referred to as "cube files".[17] They typically contain the Cartesian coordinates of atoms and a definition of the grid. The grid is defined by a starting point, three nonparallel vectors, and the size of the grid (the numbers of points in each direction defined by the grid vectors). Our software provides the following functionality: (i) identification of a CV that corresponds to a preselected value of F_e, (ii) determination of F_e associated with a given CV, and (iii) selection of a particular part of the grid limited by a predefined plane. This selection is made by zeroing the to-be-discarded part of the grid. The last functionality can be applied many times: i.e., a few planes can be defined and the grid can be trimmed to the desired slice of the orbital or the related electron density. It is up to the user to define desirable F_e's and limiting planes, if any. We believe that instructive plots of orbitals and orbital densities can be generated using the OpenCubMan software[16] in combination with molecular visualization packages and using "cube files" produced by common quantum chemistry packages.

A CV corresponding to a preselected F_e is determined using the algorithm summarized in Table 1. In this algorithm the charge density is integrated by starting from the most dense region to the least dense region. The process of density integration is stopped when a preselected fraction of the charge has been recovered. The searched CV is equal to the value of

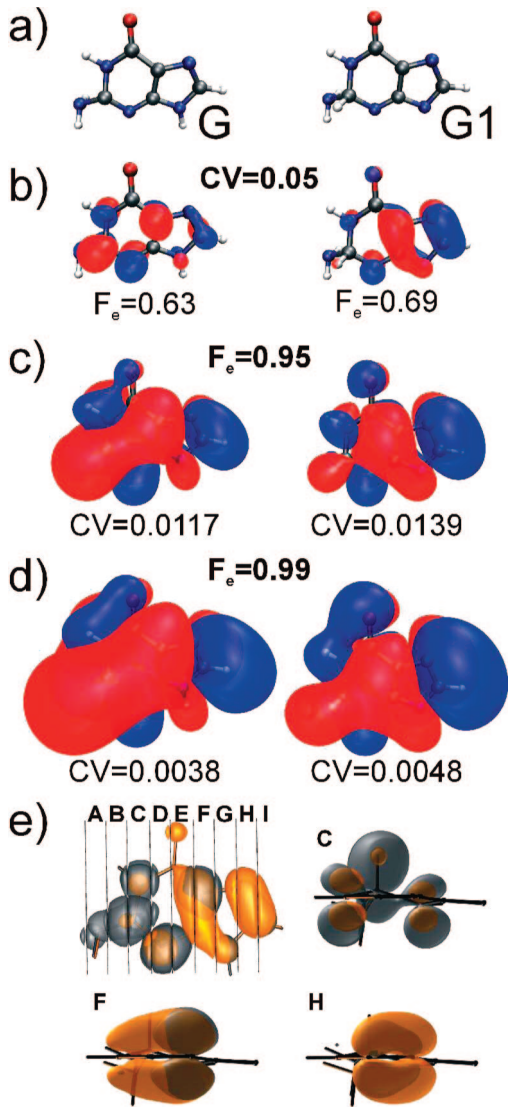

Figure 4. (a) Molecular structures of valence anions of the canonical tautomer of guanine (G) and the most stable anionic tautomer (G1). (b) Singly occupied molecular orbitals plotted using a contour value of 0.05 bohr$^{-3/2}$. (c) and (d) Singly occupied molecular orbitals plotted with F_e equal to 0.95 and 0.99, respectively. (e) Selected cross-sections of singly occupied molecular orbital densities corresponding to 0.6 e. The SOMO densities for G and G1 are superimposed and distinguished with gray and yellow, respectively. All cross-sections, marked A−I, are available in the Supporting Information (Figure S-1).

orbital density at the last integrated point (if plotting electron densities) or to the properly signed square root of it (if plotting orbitals).

Creating a cross-section of an orbital represented on a grid can be achieved by zeroing a part of the volumetric data above or below a predefined plane. A given plane is described as

$$ax + by + cz + d = 0 \tag{1}$$

where a, b, and c are components of a vector **v** normal to the plane and d is a parameter which can be calculated by solving eq 1 for a given point on the plane. A distance D of any point $p_0 = (x_0,y_0,z_0)$ from the plane can be calculated using the equation[18]

$$D = \frac{ax_0 + by_0 + cz_0 + d}{\sqrt{a^2 + b^2 + c^2}} \tag{2}$$

Such a definition allows D to have a positive or negative sign. D is positive if p_0 is on the same side of the plane as the vector **v** and negative if it is on the opposite side. When a part of the grid is zeroed by using a plane, each point of the grid is tested against eq 2, and the value of this point is set to zero or remains unchanged, if appropriate.

All of the functions presented above have been implemented in the Open-Source Cubefile Manipulator (OpenCubMan) program, which is provided free of charge under the GNU license[16] and can be downloaded from the SourceForge Internet Archive. OpenCubMan was written in the object oriented C++ programming language and is provided as a C++ object definition. OpenCubMan uses standard C/C++ libraries for all input/output operations, math, and sorting (qsort function). This form facilitates incorporating the code into other packages, libraries, or scripting languages.

The orbitals and orbital densities considered here and presented in Figures 1, 3, and 4 are based on UHF calculations for the $(ClH\cdots NH_3)^-$, $(Cl^-\cdots NH_4^+)^-$, and NH_4^0 systems as well as for the valence anions of guanine. The aug-cc-pVDZ basis set was used for all systems, with additional diffuse functions for the first three systems.[6] The "cube files" with SOMO orbitals were prepared using the Gaussian03 program.[17] They were later modified with the OpenCubMan program[16] and then visualized using the VMD software.[1]

OpenCubMan was used to determine: (i) the values of F_e corresponding to preselected CVs (Figure 1) and (ii) the values of CV corresponding to preselected values of F_e (Figures 3 and 4). The most time-consuming part of the algorithm (Table 1) is the third step, in which the values of electron density on the grid are sorted. We typically used a consistent grid of 250 × 180 × 180 points containing volumetric data for the SOMO orbitals. Sorting the electron density values on this grid took about 2 s on the available Intel Pentium 4 computer. The algorithm was also tested for a larger grid of 64 000 000 points (400 × 400 × 400) generated for the most diffuse SOMO of $(ClH\cdots NH_3)^-$. The sorting time exceeded 100 s, which is not significant in comparison with the time required to generate such a dense grid. Moreover, such extended grids are used only in very special cases, such as dipole-bound anions with very small electron binding energies. Therefore, they will not be used in typical applications.

Next, we visualized the SOMO electron densities for $(ClH\cdots NH_3)^-$, $(Cl^-\cdots NH_4^+)^-$, and NH_4^0 and three preselected values of F_e, 0.1, 0.3 and 0.5 e, and the results are presented in Figure 3. For each system we superimposed plots corresponding to the three F_e values and we created 2D cross-sections that unravel information about the relative diffuseness of the SOMO distributions. The cross-sections were produced with OpenCubMan using an approach described above. The thickness of the consecutive layers is the largest for $(ClH\cdots NH_3)^-$ and the smallest for NH_4^0, thus unraveling that the SOMO of the former is the most diffuse and that of the latter the least diffuse.

Finally we applied OpenCubMan to visualize SOMOs of valence anions of guanine. We selected the canonical tautomer (G) and the most stable anionic tautomer (G1), which we have studied in the past,[7−10] and their structures are shown in Figure

4a. When the SOMOs of G^- and $G1^-$ are visualized with the same CVs of 0.05 $bohr^{-3/2}$ (Figure 4b), then the corresponding F_e's are 0.629 and 0.694 e. Clearly, the 6.5% difference is significant, though not as large as in the $(ClH\cdots NH_3)^-$ and $(Cl^-\cdots NH_4^+)^-$ systems. The calculated electron vertical detachment energies are 0.59 and 2.43 eV or G^- and $G1^-$, respectively. We selected consistent values of F_e of 0.95 and 0.99 e, and the resulting SOMOs are shown in parts c and d of Figure 4, respectively. The plots illustrate the different bonding/antibonding character of these orbitals, which leads to different values of VDE.[19] The SOMO is more diffuse for G^- than for $G1^-$, though the differences are much smaller than for the $(ClH\cdots NH_3)^-$ and $(Cl^-\cdots NH_4^+)^-$ systems.

Finally, we show a plot that illustrates differences in the spatial distribution of the excess electron in G^- and $G1^-$. In Figure 4e and Figure S-1 (Supporting Information) we superimpose both tautomers and the corresponding SOMOs and we focus attention on nine slices, which are selected by applying specific planes. For G^-, the majority of the excess electron in localized on the six-membered ring, whereas for $G1^-$ the excess electron is localized on the five-membered ring.

In conclusion, we developed a capability to visualize molecular orbitals that differ much in the extension of charge distribution. We recommend that these plots should reproduce the same fraction of the total charge to avoid illusions that develop when constructing plots with the same contour values. The OpenCubMan software facilitates operations on common "cube files", allows superimposing molecules and associated orbitals, and selects a particular part of the orbital limited by predefined planes.

Acknowledgment. Helpful discussions with Rafał A. Bachorz and Soren Eustis are gratefully acknowledged. This work was supported by the Polish State Committee for Scientific Research Grants Nos. DS/8221-4-0140-8 (to M.G.) and N204 127 31/2963 (to M.H.). M.H. holds an award from Foundation for the Development of the University of Gdańsk (FRUG). The calculations were performed at the Academic Computer Center in Gdańsk (TASK) and at the Molecular Science Computing Facility (MSCF) in the William R. Wiley Environmental Molecular Sciences Laboratory (EMSL), where computer time was provided via a Computational Grand Challenge Project.

Supporting Information Available: Figure S-1 presenting the A−I cross sections of the SOMO densities for G^- and $G1^-$ tautomers. This material is available free of charge via the Internet at http://pubs.acs.org.

References

(1) Humphrey, W.; Dalke, A.; Schulten, K. *J. Mol. Graph.* **1996**, *14*, 33–38.

(2) Schaftenaar, G.; Noordik, J. H. *J. Comput.-Aided Mol. Design* **2000**, *14*, 123–134.

(3) Black, G.; Didier, B.; Bisethagen, T.; Feller, D.; Gracio, D.; Hackler, M.; Havre, S.; Jones, D.; Jurrus, E.; Keller, T.; Lansing, C.; Matsumoto, S.; Palmer, B.; Peterson, M.; Schuchardt, K.; Stephan, E.; Sun, L.; Taylor, H.; Thomas, G.; Vorpagel, E.; Windus, T.;Winters, C., Ecce, A Problem Solving Environment for Computational Chemistry, Software Version 3.2.5; Pacific Northwest National Laboratory, Richland, WA 99352–0999, 2006.

(4) Handy, N. C.; Marron, M. T.; Silverstone, H. J. *Phys. Rev.* **1969**, *180*, 45–48.

(5) Katries, J.; Davidson, E. R. *Proc. Natl. Acad. Sci. USA* **1980**, *77*, 4403–4406.

(6) Eustis, S. N.; Radisic, D.; Bowen, K. H.; Bachorz, R. A.; Haranczyk, M.; Schenter, G. K.; Gutowski, M. *Science* **2008**, *319*, 936–939.

(7) Haranczyk, M.; Gutowski, M. *Angew. Chem., Int. Ed.* **2005**, *44*, 6585–6588.

(8) Haranczyk, M.; Gutowski, M. *J. Chem. Inf. Model.* **2007**, *47*, 686–694.

(9) Haranczyk, M.; Gutowski, M. *J. Am. Chem. Soc.* **2005**, *127*, 699–706.

(10) Haranczyk, M.; Gutowski, M.; Li, X.; Bowen, K. H. *J. Phys. Chem. B* **2007**, *111*, 14073–14076.

(11) Howard, N. W.; Legon, A. C. *J. Chem. Phys.* **1988**, *88*, 4694.

(12) Legon, A. C. *Chem. Soc. Rev.* **1993**, *22*, 153–164.

(13) Rauk, A.; Armstrong, D. A. *Int. J. Quantum Chem.* **2003**, *95*, 683–696.

(14) Li, X.; Sanche, L.; Rauk, A.; Armstrong, D. A. *J. Phys. Chem. A* **2005**, *109*, 4591–4600.

(15) Rauk, A.; Armstrong, D. A. *Eur. Phys. J. D* **2005**, *35*, 217–224.

(16) Open-source Cubefile Manipulator Program (OpenCubMan) is available free of charge at the SourceForge archive: http://opencubman.sourceforge.net (accessed Feb 27, 2008).

(17) Frisch, M. J. ; Trucks, G. W.; Schlegel, H. B.; Scuseria, G. E.; Robb, M. A.; Cheeseman, J. R.; Montgomery, J. A., Jr.; Vreven, T.; Kudin, K. N.; Burant, J. C.; Millam, J. M.; Iyengar, S. S.; Tomasi, J.; Barone, V.; Mennucci, B.; Cossi, M.; Scalmani, G.; Rega, N.; Petersson, G. A.; Nakatsuji, H.; Hada, M.; Ehara, M.; Toyota, K.; Fukuda, R.; Hasegawa, J.; Ishida, M.; Nakajima, T.; Honda, Y. ; Kitao, O.; Nakai, H.; Klene, M.; Li, X.; Knox, J. E.; Hratchian, H. P.; Cross, J. B.; Bakken, V.; Adamo, C.; Jaramillo, J.; Gomperts, R.; Stratmann, R. E.; Yazyev, O.; Austin, A. J.; Cammi, R.; Pomelli, C.; Ochterski, J. W.; Ayala, P. Y.; Morokuma, K.; Voth, G. A.; Salvador, P.; Dannenberg, J. J.; Zakrzewski, V. G.; Dapprich, S.; Daniels, A. D.; Strain, M. C.; Farkas, O.; Malick, D. K.; Rabuck, A. D.; Raghavachari, K.; Foresman, J. B.; Ortiz, J. V.; Cui, Q.; Baboul, A. G.; Clifford, S.; Cioslowski, J.; Stefanov, B. B.; Liu, G.; Liashenko, A.; Piskorz, P.; Komaromi, I.; Martin, R. L.; Fox, D. J.; Keith, T.; Al-Laham, M. A.; Peng, C. Y.; Nanayakkara, A.; Challacombe, M.; Gill, P. M. W.; Johnson, B.; Chen, W.; Wong, M. W.; Gonzalez, C.; Pople, J. A. Gaussian 03, Revision C.02; Gaussian, Inc., Wallingford, CT, 2004.

(18) Gellert, W.; Gottwald, S.; Hellwich, M.; Kästner, H.; Künstner, H., Eds. *VNR Concise Encyclopedia of Mathematics*, 2nd ed.; Van Nostrand Reinhold: New York, 1989.

(19) Haranczyk, M.; Holliday, J.; Willett, P.; Gutowski, M. *J. Comput. Chem.*, in press (doi: 10.1002/jcc.20886).

CT800043A